

Chapter 7

Multistability in Ecosystems: Concerns and Opportunities for Ecosystem Function in Variable Environments



Ehud Meron, Yair Mau, and Yuval R. Zelnik

Abstract Ecosystems are highly nonlinear dissipative systems characterized by multiplicity of stable and unstable states. Two major concerns are associated with multistable ecosystems in variable environments. The first is related to the increased likelihood of extreme climate events at regional scales, such as droughts, floods, and heat waves, that may result in abrupt transitions to malfunctioning ecosystem states. The second concern is related to the dominant role played by humans in shaping and transforming the ecology of the Earth, and to the detrimental effects that such transformations often have. Using mathematical models of dryland ecosystems as a case study, we discuss recent advances that shed new light on these concerns. We first argue that state transitions can be gradual or incomplete rather than abrupt, providing opportunities for prevention and recovery. We further argue that analyzing the unstable states that exist along with the stable ones, identifying their existence ranges and their stable and unstable manifolds, can help to devise human intervention forms that direct ecosystems towards desired functional ecosystem states, without impairing ecosystem function. We conclude by presenting open problems and delineating further research directions.

Keywords Dryland ecosystems · Vegetation patterns · Multistability · Front dynamics · Abrupt and gradual state transitions · Human intervention

E. Meron (✉)

Blaustein Institutes for Desert Research and Physics Department, Ben-Gurion University of the Negev, Beersheba, Israel
e-mail: ehud@bgu.ac.il

Y. Mau

Department of Soil and Water Sciences, Robert H. Smith Faculty of Agriculture, Food and Environment, The Hebrew University of Jerusalem, Rehovot, Israel
e-mail: yair.mau@mail.huji.ac.il

Y. R. Zelnik

Centre for Biodiversity Theory and Modelling, Theoretical and Experimental Ecology Station, CNRS, Moulis, France
e-mail: yuval.zelnik@sete.cnrs.fr

7.1 Introduction

Ecosystems are highly nonlinear dissipative systems involving various positive feedbacks between biotic and abiotic factors [52, 60, 81]. The stabilizing effects that these feedbacks have on ecosystem states result in multiplicity of stable states in wide ranges of environmental conditions [62]. These states often include spatially periodic patterns and localized structures, in addition to spatially uniform states [59, 60]. Ecosystems, however, seldom have the time span to converge to stable asymptotic states [35]; rather, their dynamics are interrupted by natural drivers, such as droughts, fires, floods, or forest pest outbreaks, and by human intervention motivated by various functional needs, including ecosystem services, land-use changes, and restoration of degraded ecosystems.

The varying conditions that ecosystems are subjected to, natural and human driven, can induce transitions to malfunctioning states by driving ecosystems across basin boundaries, or across thresholds where stable functioning states are destabilized or disappear. These state transitions, or “regime shifts,” can be abrupt [71, 72], but are not necessarily so—they can also proceed gradually through the propagation of degradation fronts as model studies predict [3, 76, 92, 93]. Abrupt transitions involving large decline in ecosystem function are of high concern because of the projections for increased climate variability at regional scales [21, 51]. This concern is reflected by an intensive current effort to devise early-warning signals for impending abrupt transitions [41, 70]. The conditions under which state transitions are expected to be gradual rather than abrupt, and thereby provide opportunities for prevention or recovery, are far less understood.

Varying conditions can also affect the multiple *unstable states* that exist along with the stable states, changing their stable and unstable manifolds or their very existence. Understanding these states, whether they are spatially uniform, periodic, or localized, is essential for studying transient ecosystem dynamics in general [35], and transient dynamics induced by human intervention in particular. Unlike natural drivers of ecosystem change, which are erratic and unpredictable, human intervention is generally planned and controlled, and yet is often detrimental to the ecosystem in question [15, 16, 66]. Studying unstable states holds much promise for devising human intervention forms that direct ecosystem dynamics towards desired self-organized functional states. This can be achieved by identifying the growing eigenmodes associated with unstable states and studying the dynamics in the phase space they span. This approach, which puts ecosystems on tracks of self-organization towards desired ecosystem states from the start, has hardly been pursued.

Out of all contexts of ecological multistability, dryland ecosystems stand out as an excellent case study for closing the knowledge gaps mentioned above. In addition to the variety of research problems that drylands pose, related to the escalating concerns about desertification and biodiversity loss [1, 17], they show striking phenomena of vegetation pattern formation (Fig. 7.1) [14, 22, 23, 86], and they are describable by mathematical models that capture remarkably well a wide



Fig. 7.1 Aerial photographs of nearly periodic vegetation patterns in nature: (a) a spot pattern in Zambia [4], (b) a stripe pattern in Niger [86], (c) a gap (“fairy circle”) pattern in Namibia (courtesy of S. Getzin). From [59]

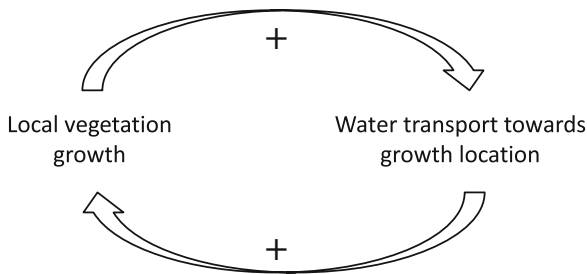


Fig. 7.2 Schematic illustration of the general positive feedback that drives vegetation pattern formation in water-limited systems. While accelerating vegetation growth in existing patches, these processes inhibit the growth in the patch surroundings, thereby favoring vegetation pattern formation. From [59]

range of observed phenomena [4, 59, 60], including multistability of uniform states, periodic patterns, and localized structures [23, 79, 92, 93].

The formation of large-scale vegetation patterns in drylands has been attributed to small-scale positive feedbacks between local vegetation growth and water transport towards the growth location, as Fig. 7.2 illustrates. Depending on the water transport mechanism, different feedbacks have been distinguished [59, 60]: (1) overland water flow induced by increased infiltration of surface water into the soil in areas of denser vegetation (infiltration feedback); (2) water conduction by laterally extended roots, the size of which increases with above-ground biomass (root-augmentation feedback); and (3) soil-water diffusion induced by strong local uptake at the vegetation-growth location and the soil-water gradients it forms (soil-water diffusion feedback). The infiltration feedback is strong in landscapes where bare soil tends to form physical or biological crusts that significantly reduce the infiltration rate relative to areas covered by vegetation [18, 23, 68]. The root-augmentation feedback is strong for plant species with high root-to-shoot ratios and laterally spread root systems [2, 24, 26]. The soil-water diffusion feedback is strong for plants with high root-to-shoot ratios and confined root systems, and for sandy soils with high hydraulic conductivities [9, 42, 93]. While these feedbacks promote local vegetation growth by drawing water from the adjacent areas of sparser vegetation, they inhibit the growth of the sparser vegetation [49, 58, 67]. This favors

nonuniform vegetation growth, or the growth of spatially periodic modes, which leads to vegetation patterns. Another pattern-forming feedback is associated with water advection, such as overland water flow on a slope [73, 75, 78] or fog advection by wind [5]. The interception of advected water by vegetation patches produces a shadowing effect on water transport in the slope or wind directions that leads to banded vegetation.

Several mathematical models have been proposed to describe vegetation pattern formation in drylands [24, 43, 48, 68, 77, 89]. These models represent a continuum modeling approach [systems of partial differential equations (PDEs)] in which the lowest level of description refers to small-scale processes rather than to individual plants, as in individual-based models [12, 13, 29]. The advantage of the continuum approach in the present context is that it lends itself to the powerful methods of pattern-formation theory. Indeed, considerable progress has been made in understanding the variety of uniform, periodic, and localized ecosystem states along the rainfall gradient, using pattern formation tools such as linear stability analysis of uniform states [26, 42, 73] and of patterned states [78, 79], derivation of amplitude (normal-form) equations [28, 87], and computation of bifurcation diagrams using numerical continuation methods [11, 76, 92, 93].

Despite the progress that has been made so far using PDE models of dryland ecosystems, many ecologically significant questions that are addressable with such models are still open or unstudied. In this paper we present and discuss open questions related to the two concerns described earlier: state transitions to malfunctioning ecosystem states and detrimental effects of human intervention.

Outline of the Chapter In Sect. 7.2, we discuss two dryland ecosystems—grasslands in western Namibia and northwestern Australia—which show striking pattern-formation phenomena and provide excellent opportunities to confront model predictions with empirical data. Since the two ecosystems feature different pattern-forming feedbacks, they are also described by different PDE models. We then use these models to address problems related to state transitions in Sect. 7.3 and to the effects of human intervention in Sect. 7.4, and describe some of the progress that has been made. We conclude by delineating directions for future research in Sect. 7.5.

7.2 The Namibian and Australian Grassland Ecosystems

Empirical testing of vegetation pattern-formation phenomena in controlled laboratory experiments is generally impractical because of the long time scales of plant growth. Remote-sensing observations provide a good alternative in fairly homogeneous and undisturbed areas, especially when the spatial scales involved are large enough to be detectable by satellite images. The availability of satellite images that go backward in time along with long-term future observations provide probes for pattern dynamics too. While vegetation pattern formation has been observed worldwide [14], two grassland ecosystems stand out in meeting the conditions of spatial homogeneity, lack of disturbances, and large spatial scales.

These are the so-called fairy circles of western Namibia [22, 40] and the recently discovered fairy circles of northwestern Australia [23]. Fairy circles are circular gaps of barren soil in grasslands that show large-scale order as Fig. 7.1c shows. The average gap diameters, 6 m in Namibia and 4 m in Australia, are large enough to be easily detectable in satellite images. The fairy circles of Namibia and of Australia show similar biomass patterns, but differ in their soil properties. In the Namibian ecosystem the soil is sandy and thus characterized by high infiltration rates of rainfall into the soil and by high hydraulic conductivities. In contrast, the top-soil layer in the Australian ecosystem is a hardly permeable claypan that generates overland water flow (runoff). As a consequence, different pattern-forming feedbacks are expected to generate the fairy-circle patterns in the two ecosystems: the soil-water diffusion feedback in Namibia and the infiltration feedback in Australia [23]. Since the plant species in both ecosystems have confined root systems, the root-augmentation feedback appears to be less significant.

In what follows, we consider the vegetation model introduced by Gilad et al. [24, 26, 60], which, unlike other models, captures all three feedbacks. The model consists of integral-partial differential equations for the areal densities of above-ground biomass $B(\mathbf{r}, t)$, soil water $W(\mathbf{r}, t)$, and overland water $H(\mathbf{r}, t)$, all in units of $[\text{kg}/\text{m}^2]$, where $\mathbf{r} = (x, y)$ [m] represents the spatial coordinates in the plane, and t [y] represents time. Depending on the dominant feedback at work, different model simplifications can be made [60]. The confined roots in both ecosystems can be used to simplify the integral terms in the general model to algebraic terms, assuming highly localized, delta-function root kernels [42]. The resulting system of three partial differential equations (PDEs) can be further simplified in studying the Namibian ecosystem, because of the high infiltration rate of sandy soil, which prevents runoff. In that case, the system of three PDEs can be reduced to a pair of PDEs for the biomass and soil-water variables [93]. The PDEs that describe the Australian and Namibian ecosystems, in dimensional forms, are as follows:

Australian Ecosystem

$$\begin{aligned}\partial_t B &= G_B B (1 - B/K) - MB + D_B \nabla^2 B, \\ \partial_t W &= IH - L_W W - G_W W + D_W \nabla^2 W, \\ \partial_t H &= P - IH - L_H H - \nabla \cdot \mathbf{J},\end{aligned}\tag{7.2.1}$$

where $\mathbf{J} = -2D_H H \nabla(H + Z)$ is the overland water flux, which depends on the ground topography function, $Z = Z(x, y)$, assumed to be independent of time (no erosion or deposition processes).

Namibian Ecosystem

$$\begin{aligned}\partial_t B &= G_B B (1 - B/K) - MB + D_B \nabla^2 B, \\ \partial_t W &= P - L_W W - G_W W + D_W \nabla^2 W.\end{aligned}\tag{7.2.2}$$

In Eqs. (7.2.1) and (7.2.2), $\nabla^2 = \partial_x^2 + \partial_y^2$ is the Laplacian in the plane, and

$$L_W = \frac{N_W}{1 + R_W B/K}, \quad L_H = \frac{N_H}{1 + R_H B/K}, \quad I = A \frac{B + Qf}{B + Q}, \quad (7.2.3)$$

$$G_B = \Lambda W(1 + EB)^2, \quad G_W = \Gamma B(1 + EB)^2, \quad (7.2.4)$$

are, respectively, the rates of soil-water evaporation, overland water evaporation, infiltration, biomass growth, and water uptake. The quantity P [mm/y] represents the precipitation rate, K [kg/m²] represents late-growth species-specific biomass constraints, such as stem strength for woody vegetation or maximal attainable biomass in the life cycle of annuals, and E [m²/kg] represents the root-to-shoot ratio. In obtaining Eq. (7.2.2) we assumed a flat or mildly sloped terrains that do not induce overland water flow. We note that the specific biomass dependence of G_B and G_W in Eq. (7.2.4) follows from a root architecture described by a Gaussian root kernel in the original model [60]. Other choices of root distributions can lead to different forms for G_B and G_W . Information about the remainder of the parameters and about non-dimensional forms of the model equations can be found in Refs. [23, 59, 60]. Although we refer here to two particular ecosystems involving herbaceous vegetation, the models are more general and applicable to woody vegetation as well.

Out of the three pattern-forming feedbacks, the Namibian ecosystem model captures only the soil-water diffusion feedback. The strength of this feedback is controlled by the root-to-shoot ratio E and by the soil-water diffusivity D_W ; increasing any of these parameters strengthens the feedback, as it acts to increase soil-water diffusion towards vegetation patches. The Australian ecosystem model captures in addition the infiltration feedback; a strong feedback is obtained with sharp infiltration contrast $f \ll 1$ (see I in Eq. (7.2.3)) and large runoff transport coefficient D_H , as both act to speed up overland water flow. The two feedbacks suggest different spatial distributions of soil-water with respect to biomass: anti-phase distributions (maxima of biomass coincide with minima of soil water) in the case of the soil-water diffusion feedback, and in-phase distributions in the case of the infiltration feedback. A linear stability analysis of the uniform vegetation state indeed confirms these expectations [42]. In the Namibian ecosystem, where the soil-water diffusion feedback appears to be the dominant one, the distributions are expected to be anti-phase. A recent empirical study indeed supports this expectation [8]. An additional support for the soil-water diffusion feedback comes from another recent study according to which lateral water transport in the soil occurs over distances as large as 7.5 m, which is consistent with the typical length scale associated with the fairy circles [9]. In the Australian ecosystem the infiltration feedback is the dominant one, because of the claypan top layer that forms a hardly permeable soil crust. As overland water infiltrates mostly in vegetation patches, the biomass and soil-water distributions are likely to be in-phase [23]. An additional biomass-water feedback captured by the model equations for both ecosystems is

associated with reduced evaporation in vegetation patches, hereafter the “shading feedback.” This is a positive but non-pattern-forming feedback because it does not involve water transport. Yet, it plays an important role in inducing multiple stable states as we discuss below.

It should be noted that an alternative explanation of the fairy-circle phenomenon has been proposed, according to which the circles represent foraging areas of termite nests [40, 83]. The termite hypothesis, however, does not explain the fairy circles of Australia, where termite nests were found to be uncorrelated to the circles [23]. The correlations that have been found between rainfall patterns and fairy-circle dynamics in Namibia [22, 93], the occurrence of Namibian fairy circles within a narrow rainfall range between the 70 and 120 mm/y isohyets [22], and observations of fairy circles with no termite colonies also in Namibia [65], pose additional challenges to the termite hypothesis.

The general Gilad et al. model [26] and its two simplified versions (7.2.1) and (7.2.2) show a universal sequence of basic vegetation states along the rainfall gradient as Fig. 7.3 illustrates [28, 50, 59, 68, 89]: bare soil, hexagonal spot pattern, stripe pattern, hexagonal gap pattern, and uniform vegetation. The emergence of gap patterns from uniform vegetation and the morphology changes that these patterns go through as rainfall decreases, first to stripe patterns and then to spot patterns, represent a population-level mechanism to cope with water stress. By self-organizing in spatial patterns the vegetation benefits not only from direct rainfall, but also from water transport towards vegetation patches from the surrounding bare-soil patches. In the Namibian ecosystem water is transported mainly by soil-water diffusion [9, 65, 93], whereas in the Australian ecosystem the transport is mainly through overland water flow [23]. With further rainfall decrease the water-contributing bare-soil areas should increase in size to compensate for the lower rainfall, which drives the two morphological changes mentioned above. Both the Namibian and Australian ecosystems show strikingly regular gap patterns (Fig. 7.1c). Statistical analyses of these patterns, including the calculation of pair-correlation functions, show a dominating hexagonal order, where each gap is surrounded on average by six equidistant gaps, as the models predict [22, 23].

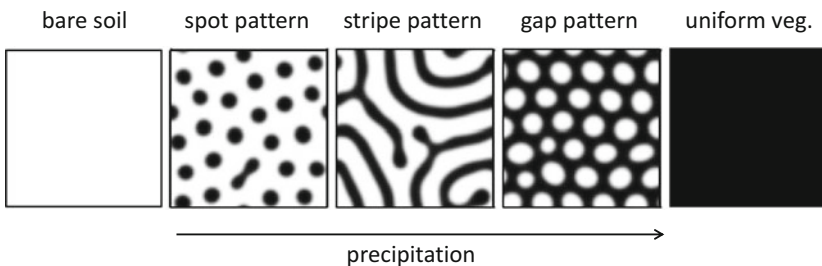


Fig. 7.3 The five basic vegetation states along the rainfall gradient as obtained by model simulations; uniform vegetation, hexagonal gap pattern, stripe pattern, hexagonal spot pattern, and bare soil. From [59]

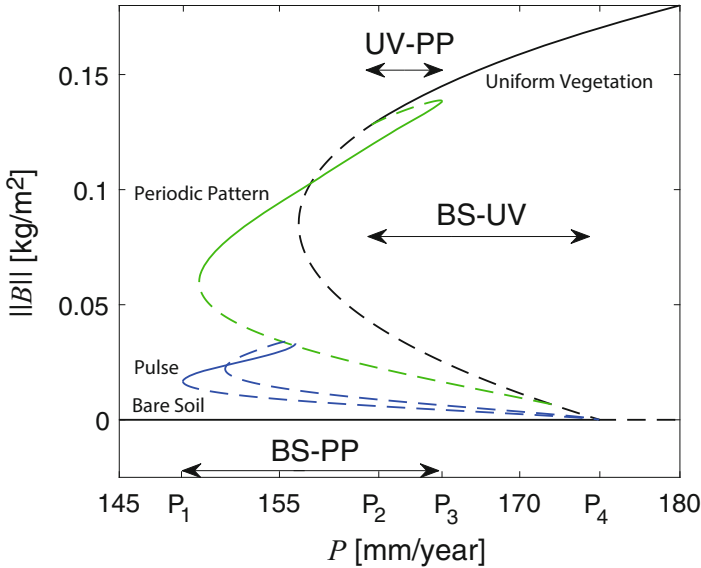


Fig. 7.4 Bifurcation diagram showing different types of bistability ranges along the rainfall gradient. The diagram shows four solutions of the Namibian ecosystem model (7.2.2) in 1d, representing bare soil, uniform vegetation, periodic vegetation pattern, and a single vegetation patch (pulse). The vertical axis is the L^2 norm of the biomass variable, while the horizontal axis represents the precipitation rate. Solid (dashed) lines represent stable (unstable) solutions. The thresholds P_4 , P_3 , P_2 , P_1 denote, respectively, the uniform instability of bare soil, the appearance of periodic patterns in a saddle-node bifurcation, the nonuniform instability of uniform vegetation, and the disappearance of isolated vegetation patches, represented by a pulse solution, in a saddle-node bifurcation. The horizontal double arrows represent three types of bistability ranges: (1) bare soil and uniform vegetation, BS-UV ($P_2 < P < P_4$), (2) uniform vegetation and periodic patterns, UV-PP ($P_2 < P < P_3$), and (3) bare soil and periodic patterns, BS-PP ($P_1 < P < P_3$). The latter range includes periodic patterns made of weakly interacting pulses. Note that the UV-PP bistability range is, in fact, a tristability range as the bare-soil solution is also stable

The model Eqs. (7.2.1) and (7.2.2) also predict several forms of multiple stable states along the precipitation axis, associated with the positive biomass-water feedbacks that the equations capture. Figure 7.4 shows a bifurcation diagram that illustrates three types of bistability ranges. The simplest form is bistability of bare soil and (spatially) uniform vegetation (BS-UV in Fig. 7.4), which results from a uniform (zero wavenumber) imperfect pitchfork bifurcation [59, 82] of bare soil to uniform vegetation ($P = P_4$ in Fig. 7.4). Note that the negative-biomass solution is discarded as it does not represent a physical state. This bistability range can be realized with high evaporation rates in bare soil, which stabilize the bare-soil solution up to precipitation values where uniform vegetation is also a stable solution. In the Namibian ecosystem model these conditions can be realized when the soil-water evaporation is fast relative to water uptake and vegetation growth. In the model for the Australian ecosystem the condition for bare-soil stabilization can be realized with a high evaporation rate of overland water relative to the infiltration rate [23].

Such a high evaporation rate is consistent with observed surface temperatures in bare soil, which can be as high as 75°C [23].

Besides bistability of uniform states, two main bistability forms that involve uniform and patterned states, are possible: bistability of uniform vegetation and periodic patterns—hexagonal gap patterns in two spatial dimensions (2d) (UV-PP in Fig. 7.4), and bistability of bare soil and periodic patterns—hexagonal spot patterns in 2d (BS-PP in Fig. 7.4). These bistability forms are obtainable with strong pattern-forming feedbacks that lead to subcritical nonuniform (finite-wavenumber) instabilities of uniform vegetation [59], and act to stabilize the patterned states once they are formed. In the Australian ecosystem model (7.2.1) this is the infiltration feedback (small f), while in the Namibian ecosystem model (7.2.2) it is the soil-water diffusion feedback (large E and D_W/D_B). A third bistability form involving uniform and patterned states is possible under conditions of weak shading feedback (small R_W and R_H in Eq. (7.2.3)) in addition to a strong pattern-forming feedback. In that case, the instability of bare soil to uniform vegetation is supercritical, resulting in a stability range of uniform low-biomass vegetation as Fig. 7.10 shows.

Conditions that give rise to both bistability of bare soil and uniform vegetation and bistability of uniform vegetation and periodic patterns result in a tristability range of uniform vegetation, periodic patterns, and bare soil (see Fig. 7.4). Indeed, aerial images of fairy circles in Australia reveal mixtures of nearly periodic gap patterns and large bare-soil areas, suggesting the possible stability of both states [23]. In the next section we discuss possible implications of these multistability forms to state transitions.

7.3 Abrupt vs. Gradual State Transitions

Underlying the view of regime shifts as abrupt state transitions is the presumption that these transitions are global, encompassing the whole system. This view does not take into account the spatial confinement of most disturbances, such as clear-cutting, grazing, fires, or infestation, which often induce local state transitions, rather than global transitions. The dynamics that follow local state transitions crucially depend on the transition zones that separate the two alternative stable states. These zones are fronts whose structures and dynamics have thoroughly been studied in various pattern formation contexts [10, 32, 36, 59, 63]. Depending on the dynamics of a single front, on the interactions between adjacent fronts, and on instabilities that fronts may go through, different asymptotic states can result.

We begin by discussing the simpler case of bistability of uniform states. In the context of dryland ecosystems, bistability of two uniform states can be realized in precipitation ranges where both uniform vegetation and bare soil are stable states (see Fig. 7.4). In this case fronts generically propagate. A particular control-parameter value may exist for which the front is stationary, often called the Maxwell point, but any deviation from this value results in front motion [59]. A simple example can illustrate these general results. Consider the equation

$$\partial_t u = \lambda u + \alpha u^2 - u^3 + \partial_x^2 u. \quad (7.3.1)$$

For $\alpha > 0$ the zero solution goes through a subcritical pitchfork bifurcation at $\lambda = 0$ that results in bistability range, $-\alpha^2/4 < \lambda < 0$, of the zero solution and the nonzero solution, $u_+ = \alpha/2 + \sqrt{(\alpha/2)^2 + \lambda} > 0$. Within this range propagating front solutions that are biasymptotic to the two states exist, e.g., $u \rightarrow 0$ as $x \rightarrow -\infty$ and $u \rightarrow u_+$ as $x \rightarrow \infty$. The front speed, c , of a propagating front is uniquely determined by the parameters λ and α [59] and can be calculated by considering constant-speed fronts. Inserting $u(x, t) = u(x - ct)$ into Eq. (7.3.1) we obtain

$$\frac{d^2 u}{dz^2} + c \frac{du}{dz} - \frac{dV}{du} = 0, \quad (7.3.2)$$

where $z = x - ct$ and

$$V = -\frac{\lambda}{2}u^2 - \frac{\alpha}{3}u^3 + \frac{1}{4}u^4 + V_0 \quad (7.3.3)$$

is a double-well potential with minima $V_0 = V(0)$ and $V_+ = V(u_+)$ at the zero and nonzero solutions. Multiplying Eq. (7.3.2) by du/dz and integrating we find

$$c \propto \int_{-\infty}^{\infty} \frac{dV}{du} \frac{du}{dz} dz = \int_0^{u_+} \frac{dV}{du} du = V_+ - V_0. \quad (7.3.4)$$

The Maxwell point corresponds to the value $\lambda = \lambda_M = -2\alpha^2/9$ at which $V_+ = V_0$, i.e., to a stationary front. Clearly, any deviation from the Maxwell point results in wells of different depth and, consequently, in front motion.

A consequence of the generic property of front propagation is that domains of one stable state embedded in the second stable state either shrink or expand. In the course of time the fronts that bound these domains approach one another, their tails begin to overlap and the fronts interact [36]. When these interactions are attractive, as in the particular example given by Eq. (7.3.1), expanding domains coalesce into bigger ones by front annihilation. In that case, a disturbance that results in an expanding domain of a given state will eventually lead to a global transition to this state, but in a gradual manner—by front propagation. Note that such a transition can take place anywhere from the Maxwell point to the edge of the bistability range or the tipping point where an abrupt global transition occurs [3]. Global transitions of this kind are also possible with weak repulsive front interactions, but when the interactions are strong enough the fronts may come to a stop rather than annihilate [27, 32]. In the case of Eq. (7.2.2), repulsive front interactions can prevent a global transition from uniform vegetation to bare soil, as Fig. 7.5 illustrates. Repulsive interactions result from reduced competition for water in diminishing vegetation domains. When these interactions are strong enough the asymptotic state is not uniform, but rather a spatial pattern. That pattern consists of large bare-soil domains separated by vegetation stripes, and reflects a partial regime shift [59, 91].

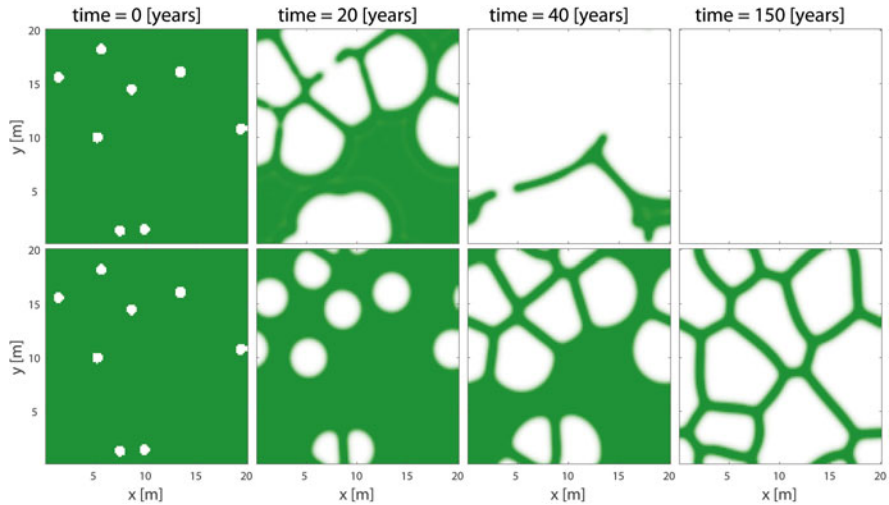


Fig. 7.5 Global vs. partial gradual regime shifts. Shown are the dynamics of a locally disturbed uniform vegetation state, obtained by solving Eq. (7.2.2) numerically in 2d at two precipitation values that are sufficiently below the Maxwell point, where small bare-soil domains expand into the surrounding vegetation areas. Top row: $P = 165$ [mm/y], far below the Maxwell point, where fast expansion of initially small bare-soil domains eventually leads to a global shift to uniform bare soil. Bottom row: $P = 170$ [mm/y], closer to the Maxwell point, where bare-soil domains expand more slowly and repulsive front interactions result in a partial regime shift to large bare-soil domains separated by narrow vegetation stripes. See Ref. [91] for additional information. From [91]

Fronts in bistable systems may go through two general types of instabilities, transverse and longitudinal, as Fig. 7.6 illustrates for an activator-inhibitor type system [59]. Transverse instabilities involve front-structure changes along the front line [27, 30], such as curvature modulations (Fig. 7.6a). By contrast, longitudinal instabilities involve changes normal to the front, e.g., a change in the position of an inhibitor front relative to an activator front. A good example is the so-called Nonequilibrium Ising-Bloch (NIB) bifurcation [7, 32]. In a bistable system with an inversion symmetry, this is a pitchfork front bifurcation in which a stationary (Ising) front is destabilized to a pair of counter-propagating (Bloch) fronts [7, 31, 32, 39, 61] (Fig. 7.6b). Although front instabilities are local processes, occurring in the confined front zone, their influence usually extends to the entire system. A transverse instability results in the growth of fingers that split at their tips into new fingers, which grow and tip-split again until the entire system is filled up with a stationary labyrinthine pattern (Fig. 7.6a) [27, 30]. Note that this process requires repulsive front interactions to prevent the coalescence of adjacent fingers into larger domains. A longitudinal instability, such as the NIB bifurcation, can result in counter-propagating front segments that develop in the course of time into space-filling spiral waves [31, 33, 53]. In both types of front instability the asymptotic state is a spatial pattern, either stationary or time dependent, rather than an alternative uniform state.

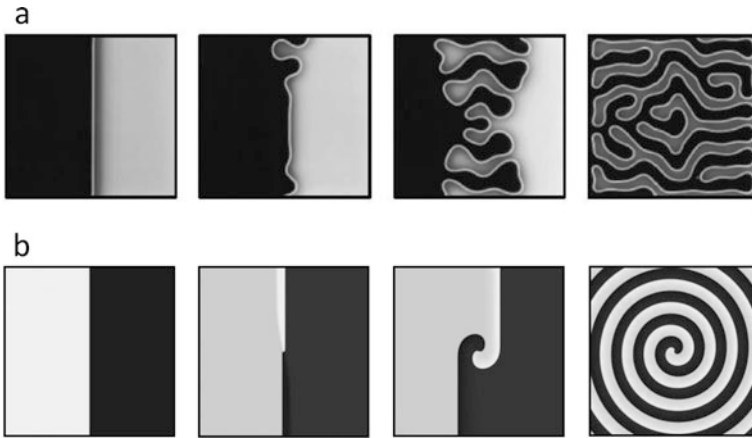


Fig. 7.6 Local front instabilities can lead to global patterns. Shown are snapshots of numerical simulations of a FitzHugh–Nagumo model (time proceeds from left to right) that illustrate transverse (**a**) and longitudinal (**b**) front instabilities, and the asymptotic patterns they lead to—labyrinthine pattern and spiral wave, respectively. Further details in Ref. [30]. From [59]

Front instabilities may well be found in models of dryland vegetation as these are also activator-inhibitor systems showing bistability of uniform states (UV and BS), where biomass is the activator and lack of soil-water—the inhibitor [44]. Front dynamics in bistability of uniform vegetation and bare soil have received little attention so far [20, 76]. Further studies are needed to test the relevance of incomplete regime shifts, driven by repulsive front interactions and front instabilities, to real ecosystems, such as the Namibian and the Australian ecosystems discussed in Sect. 7.2.

More attention has been devoted to the two bistability forms of uniform and patterned states: uniform vegetation and periodic gap patterns, and periodic spot patterns and bare soil [6, 11, 74, 79, 80, 92–95]. According to pattern-formation theory, and in contrast to bistability of uniform states, when one of the alternative states is a periodic pattern, fronts can be stationary or pinned in a *range* of the control parameter [64]. In this range alternative-state domains can remain fixed in size, neither expanding nor retracting, forming a multitude of stable hybrid states. The latter can be spatially localized, representing single alternative-state domains of different sizes, or spatially extended, corresponding to various combinations of localized domains. In a bifurcation diagram, such as that shown in Fig. 7.7 for the Namibian ecosystem model, localized hybrid states appear as solution branches that snake back and forth as the sizes of the domains they represent change, a behavior that has been termed “homoclinic snaking” [45, 46]. The snaking solution branches occupy a subrange of the bistability range—the snaking range. Thus, three front types can be distinguished in a bistability range of uniform and patterned states: a stationary pinned front within the snaking range and two fronts moving in opposite directions on either side of this range. Local disturbances within a snaking range

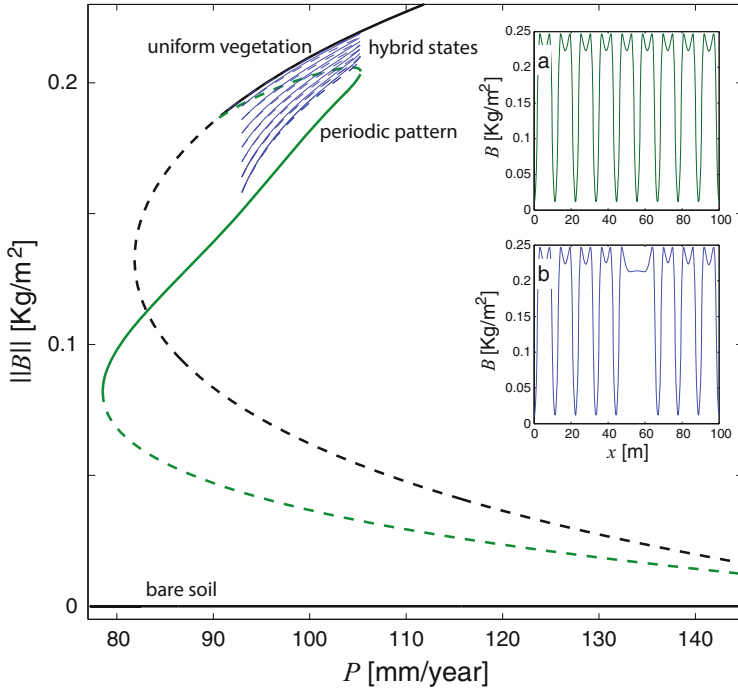


Fig. 7.7 Bifurcation diagram for the Namibian ecosystem model (7.2.2) in 1d. The vertical axis is the L^2 norm of the biomass variable. Solid (dashed) lines represent stable (unstable) solutions. The diagram shows a precipitation (P) range where both uniform vegetation and periodic vegetation pattern are stable. Within this range there exists a subrange of hybrid states. The insets show spatial profiles of a 1d periodic gap pattern (a) and of a hybrid state consisting of a periodic gap pattern with a missing gap, i.e., with the smallest domain of the alternative uniform vegetation state (b). From [59]

should have little effect as the fronts are stationary and initial alternative-state domains quickly converge to nearby hybrid states. Local disturbances outside the snaking range, but still inside the bistability range, result in gradual shifts. Gradual shifts may also occur within the snaking range when the system is subjected to environmental fluctuations. Such fluctuations, if strong enough, can kick the system temporarily outside the snaking range, where fronts do propagate, and thereby induce hybrid-state transitions that gradually shift the system towards the alternative stable state [3, 93]. The wider the snaking range the more resilient the system is to environmental fluctuations and local disturbances. Identifying the biotic and abiotic parameters that control the width of the snaking range relative to the bistability range is therefore a highly significant unstudied problem.

Hybrid states are likely to exist in the Namibian ecosystem, as the satellite images in Fig. 7.8 suggest [93]. Finding empirical evidence for hybrid-state transitions and gradual regime shifts is more intricate. The closest evidence comes from studies of fairy-circle “birth” and “death” events [85], which have been interpreted recently

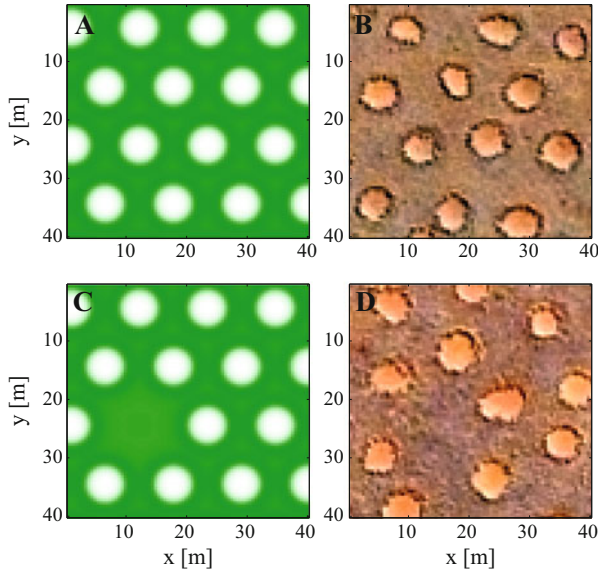


Fig. 7.8 Patterned states in the Namibian ecosystem. Hexagonal gap pattern obtained by integrating the Namibian ecosystem model (7.2.2) in 2d (a), and a satellite image showing a similar nearly hexagonal pattern of fairy circles in western Namibia (b). A hybrid state consisting of one missing gap obtained from the model (c), and a similar hybrid state obtained from a satellite image (d). Adapted from [93]

as hybrid-state transitions induced by rainfall variability [93]. Figure 7.9a shows satellite images that span a period of 10 years and demonstrate the birth of a fairy circle after a severe drought in 2007. Figure 7.9b shows a simulation of the Namibian ecosystem model, using the first satellite image in 2004 as an initial condition with a precipitation value within the snaking range, and mimicking the 2007 drought by a precipitation downshift that takes the system outside the snaking range for a period of 1 year. As the simulation snapshots show, a new gap has appeared after a 10-year period, exactly at the same location where the actual fairy circle has appeared. The simulated temporal escape from the snaking range that was needed to induce the formation of the new gap supports the view of fairy-circle birth events as hybrid-state transitions. A series of droughts can result in a cascade of hybrid-state transitions and a gradual shift [93], but empirical evidence for such a cascade has not been reported yet.

Homoclinic snaking can also be found in a bistability range of low-biomass uniform vegetation and periodic spot pattern, as Fig. 7.10 shows [11], implying the feasibility of hybrid-state transitions and gradual shifts in fluctuating environments. However, when the periodic-pattern solution branch extends to the stability range of the bare-soil state, homoclinic snaking breaks down in what appears to be a Belyakov–Devaney transition [38]. In that case shifts from periodic patterns to bare soil, or desertification, are found to be abrupt [95]. While most model studies predict

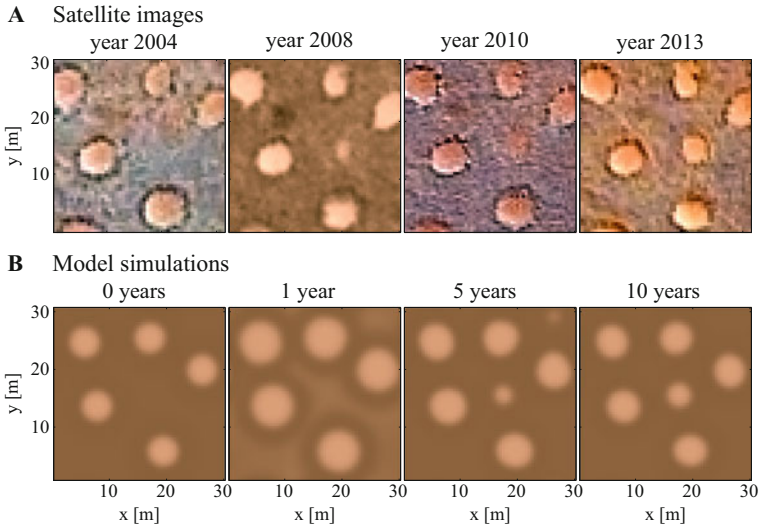


Fig. 7.9 Birth of fairy circles as a hybrid-state transition. (a) Satellite images showing the birth of a new fairy circle. (b) Snapshots of model simulations [Eq. (7.2.2)], using initial conditions derived from the 2004 satellite image (first snapshot from left) and mimicking a 1-year drought (second snapshot from left), which show similar fairy-circle birth dynamics. Adapted from [93]

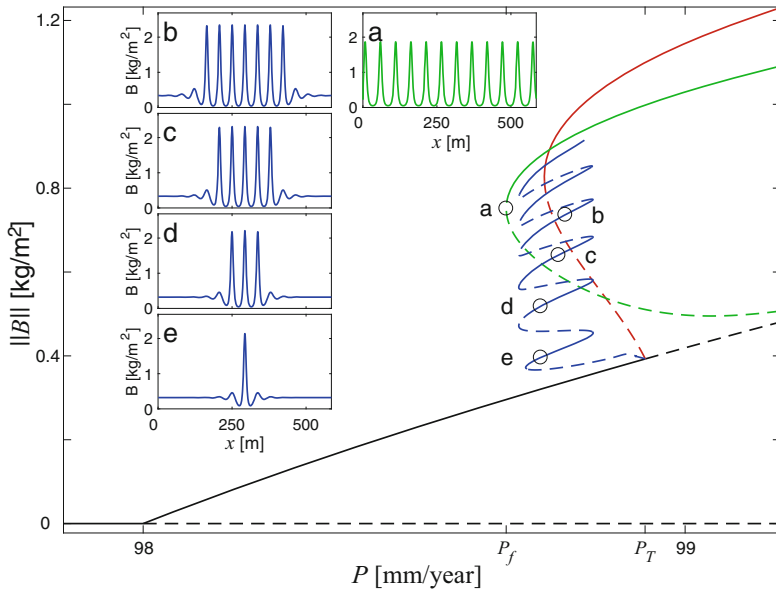


Fig. 7.10 Bifurcation diagram for the Australian ecosystem model (7.2.1) in 1d with weak shading feedback (small R_W and R_H in (7.2.3)). The diagram shows a small bistability range, $P_f < P < P_T$, of low-biomass uniform vegetation (black line) and a periodic pattern (green line) and a subrange of homoclinic snaking. The inset (a) shows the periodic solution while the insets (b–e) show localized pattern solutions or hybrid states

wide bistability ranges of spot patterns and bare soil, and thus the likelihood of abrupt desertification, these studies have been confined to a single species. Quite often dryland landscapes consist of woody and herbaceous species, forming a bistability range of woody spot patterns and uniform herbaceous vegetation [25]. Studies of two-species models do predict homoclinic snaking [47], suggesting that the degradation of woody spot patterns may be gradual rather than abrupt.

In the tristability range of bare soil, periodic patterns, and uniform vegetation [see Fig. 7.7] many front types are expected to coexist, pinned, or moving; fronts separating domains of uniform vegetation and bare soil, domains of uniform vegetation and periodic patterns, and domains of periodic patterns and bare soil. The dynamics, interactions, and stability properties of these front solutions, and the implications for regime shifts have hardly been studied [96].

7.4 Human Intervention Along Unstable Eigenmodes

The dominant role played by humans in shaping and transforming the ecology of the Earth is well recognized [19]. More than three-quarters of the terrestrial biosphere have already been transformed into anthropogenic biomes by human populations and this trend is intensifying. A major question that arises in this regard is how to intervene in ecosystem dynamics so as to achieve the intervention goal without harming ecosystem function. While this question appears to be overwhelmingly hard in many contexts of human intervention, it may be tractable for selected contexts that are simple enough to be modeled mathematically and yet ecologically significant. In the following we focus on a specific example of such a context, vegetation restoration in fluctuating environments, and use it to illustrate a general approach to human intervention that highlights the roles of unstable states.

A common restoration practice is water harvesting by spatially periodic ground modulations, such as parallel micro-catchments, that capture overland water flow and along which vegetation is planted [88]. This is a spatial resonance problem where a system that tends to form a periodic pattern with a preferred wave-number k_0 is forced to follow an external template with a different wave-number k_f . The question we wish to address here is the following: given a stripe-like template of ground modulations in the x direction, characterized by a wave-vector $\mathbf{k}_f = (k_f, 0)$, what should be the vegetation-planting pattern in order to achieve the restoration goal of establishing a bio-productive state that remains functional in a fluctuating environment?

We address this question using Eq. (7.2.1), modified to include a periodically modulated infiltration rate to mimic periodic soil-crust removal, a lighter and more cost-effective intervention form than micro-catchments [56],

$$I(B) = A \frac{B + Qf}{B + Q}, \quad f = f_0 \left[1 + \frac{\gamma_f}{2} (1 + \cos(k_f x)) \right], \quad (7.4.1)$$

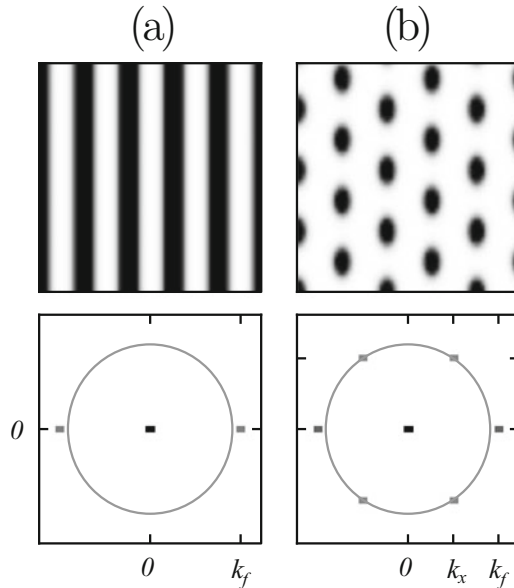


Fig. 7.11 Resonant responses to stripe-like ground modulations with wave-vector $\mathbf{k}_f = (k_f, 0)$. Top panels: a resonant stripe pattern (a) and a resonant rhombic pattern (b) in the x (horizontal) and y plane, obtained by numerical integration of Eqs. (7.2.1) and (7.4.1). Dark shades denote high biomass. Bottom panels: the corresponding Fourier transforms (in absolute value), where darker dots denote higher absolute values, and the circle $|\mathbf{k}| = k_0$. The peaks at $\pm \mathbf{k}_f$ and the absence of peaks on the circle of radius k_0 in (a) indicate that the stripe pattern is in 1:1 resonance with the forcing. The four peaks on the circle of radius k_0 in (b) represent the two oblique modes, $\mathbf{k}_{\mp} = (-k_x, \mp k_y)$, and their complex conjugates, $-\mathbf{k}_{\mp}$. The value $k_x = k_f/2$ indicates that the rhombic pattern is 2:1 resonance with the forcing. From [56]

where $f_0 \ll 1$ is the infiltration contrast of an unmodulated soil and γ_f represents the modulation strength. According to this form the infiltration rate in a densely vegetated area is high, $I \approx A$, because the biomass density there is significantly higher than Q , a species-dependent reference value representing an over 50% increase of the infiltration rate, whereas in bare soil it is much lower, $I = Af_0$ in unmodulated bare soil and $I = (1 + \gamma_f)Af_0$ in bare soil with removed crust. Figure 7.11 shows two types of resonant patterns and the absolute values of their Fourier transforms: (a) a stripe pattern that locks to the forcing in a 1:1 resonance (vegetation stripe at each ground modulation), (b) a rhombic pattern that locks to the forcing in a 2:1 resonance (vegetation spot at every second ground modulation). The Fourier transforms show the basic modes that constitute these patterns; a stripe mode, $\mathbf{k} = \mathbf{k}_f = (k_f, 0)$, in the case of a stripe pattern (and its conjugate mode $(-k_f, 0)$), and three modes in the case of a rhombic pattern, a stripe mode, $\mathbf{k}_f = (k_f, 0)$, and two oblique modes, $\mathbf{k}_{\pm} = (k_x, \pm k_y)$, where $k_x = k_f/2$ and k_y are such that the total wave-number k is equal to the preferred wave-number k_0 , i.e., satisfies $k^2 = k_x^2 + k_y^2 = k_0^2$. Note that the three wave-vectors \mathbf{k}_f and \mathbf{k}_{\pm} satisfy the

resonance relation, $\mathbf{k}_f + \mathbf{k}_+ + \mathbf{k}_- = 0$, which drives the simultaneous growth of the three modes, and that in the case of an exact resonance ($k_f = k_0$) the rhombic pattern becomes a hexagonal pattern consisting of three wave-vectors 120° apart. Numerical studies of Eqs. (7.2.1) and (7.4.1) reveal a bistability range of resonant stripe and rhombic patterns and that rhombic patterns extend to lower precipitation values than stripe patterns [56].

Both stripe and rhombic patterns represent productive states, and establishing any one of them would satisfy the restoration goal. The larger area of vegetation coverage in the case of stripe patterns does not necessarily imply higher total biomass or productivity, because of the larger water-contributing areas in the case of rhombic patterns, which results in higher biomass densities in the vegetation patches. The remaining question is which of the two patterns is more resilient to droughts, and thus better functioning in fluctuating environments? Figure 7.12 shows the response of resonant stripe patterns to a moderate precipitation downshift, which results in convergence to a rhombic pattern (top row), and to a stronger downshift, which results in collapse to bare soil (bottom row) despite the existence of stable rhombic patterns. The same numerical experiment conducted with an initial rhombic pattern results in no significant pattern change. These results suggest that stripe patterns are less resilient to droughts than rhombic patterns.

In order to understand the mechanism of collapse to bare soil let us focus on the amplitudes A , a_+ , a_- of the stripe and the two oblique modes, respectively, in terms of which the state variables $U = (B, W, H)$ can be approximated as

$$U(\mathbf{x}, t) \approx U_0 + U_1 A e^{ik_f x} + U_2 a_+ e^{i\mathbf{k}_- \cdot \mathbf{r}} + U_3 a_- e^{i\mathbf{k}_+ \cdot \mathbf{r}} + \text{c.c.}, \quad (7.4.2)$$

where U_0 , U_1 , U_2 , U_3 are constant vectors, and we assumed proximity to the bare-soil instability and weak ground modulations. Equations for the amplitudes A , a_+ ,

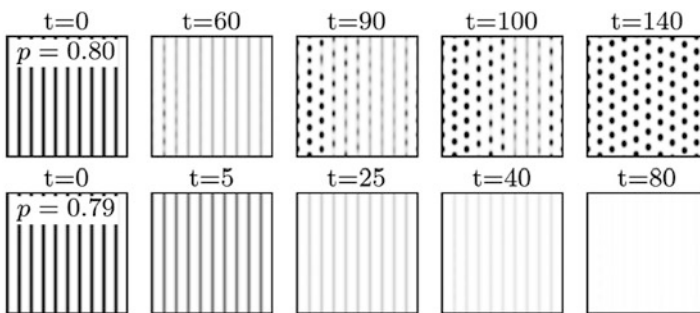


Fig. 7.12 Resilience of stripe patterns to droughts. Numerical simulations of Eqs. (7.2.1) and (7.4.1) showing the response of a resonant stripe pattern, obtained at a precipitation value within the bistability range of stripe and rhombic patterns, to precipitation downshifts of different strength to a range where rhombic patterns are still stable. The response to a moderate downshift results in quick convergence to a rhombic pattern (top row), while the response to a stronger downshift results in collapse to bare soil. Adapted from [56]

a_- have been derived for a simple pattern-formation model, the Swift–Hohenberg equation with parametric spatial forcing [54–56]. Derivation of amplitude equations for the vegetation model (7.2.1) and (7.4.1) is harder and has not been done yet. However, because of the universal character of amplitude equations we may expect their general form to apply to the restoration problem as well. Indeed, the amplitude equations can produce a bifurcation diagram similar to that found by numerical integration of the vegetation model [56], interpreting the bifurcation parameter as the precipitation rate P . In the following we use these amplitude equations to study the response to precipitation downshifts. A schematic form of the diagram obtained from the amplitude equations is shown in Fig. 7.13.

Consider two precipitation downshifts of different strengths, applied to stable stripe patterns as the arrows in Fig. 7.13 indicate: a moderate downshift to P_2 where stripe solutions exist but are unstable (green arrow), and a stronger downshift to P_1 where stripe solutions do not exist (red arrow). Note that both downshifts take the system to a precipitation range where rhombic patterns are still stable solutions and significantly far from the saddle-node bifurcation at which they disappear. Figure 7.14 shows the phase planes spanned by the amplitude moduli $\rho_S = |A|$ and $\rho_R = |a_+| = |a_-|$ at P_2 and P_1 , where we took advantage of the symmetry between the two oblique modes in the precipitation range we consider. Shown in

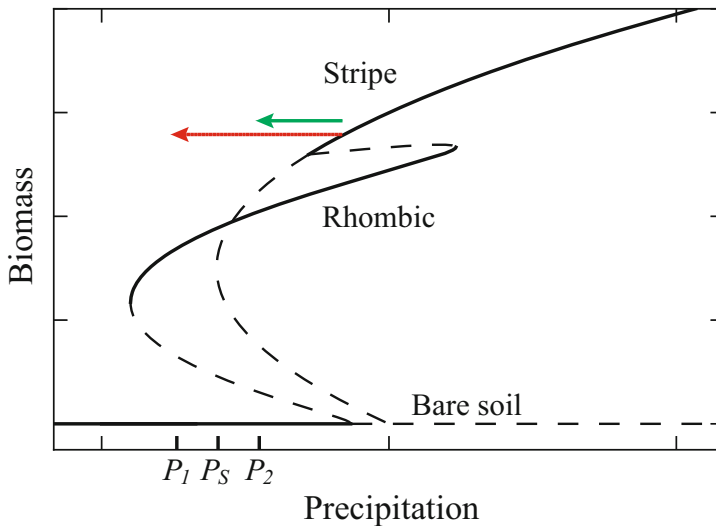


Fig. 7.13 A schematic bifurcation diagram for vegetation restoration. The solution branches describe bare soil, stripe pattern, and rhombic pattern, where solid (dashed) lines denote stable (unstable) solutions. The vertical axis represents the L^2 norm of the biomass expressed in terms of the modes’ amplitudes, $\sqrt{|A|^2 + |a_+|^2 + |a_-|^2}$. The precipitation value P_S denotes the disappearance of unstable stripe solutions in a saddle-node bifurcation. The green and red arrows represent precipitation downshifts from the stability range of stripe patterns to precipitation values $P_2 > P_S$ and $P_1 < P_S$, respectively. Adapted from [56]

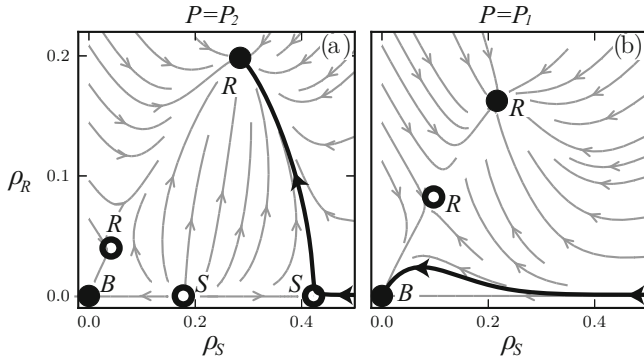


Fig. 7.14 Phase-space dynamics in the plan spanned by $\rho_S = |B|$ and $\rho_R = |a_{\pm}|$ at (a) $P = P_2$, where a pair of unstable stripe solutions exists, (b) at $P = P_1$, where the unstable stripe solutions no longer exist (see Fig. 7.13). The solid (hollow) circles denote stable (unstable) stationary states. The labels B , S , and R denote the bare-soil state, stripe patterns, and rhombic patterns, respectively, and the arrows denote the vector field of the amplitude equations. The responses of a stable resonant stripe pattern to precipitation downshifts are shown by the thick black phase portraits: (a) A moderate shift to a range where unstable stripe solutions still exist, results in a smooth transition to a rhombic pattern. (b) A stronger shift to a range where stripe solutions no longer exist, results in a collapse to bare soil. Adapted from [56]

these phase planes are the stationary uniform and patterned states (fixed points) that exist at the respective precipitation value, and their stability properties. Also shown in Fig. 7.14 are phase trajectories (black lines) of numerical solutions of the amplitude equations, starting with stripe solutions that were computed at a higher P within their range of stability. A moderate downshift to P_2 results in a smooth transition to a rhombic pattern as Fig. 7.14a shows. The unstable large-amplitude stripe solution plays a crucial role in this response; its unstable manifold, which represents the growth of the two oblique eigenmodes, acts as a barrier for the flow in phase space and prevents convergence to the stable bare-soil solution. By contrast, a stronger downshift to P_1 results in collapse to bare soil, as the stripe solution and its unstable manifold no longer exists to constrain the phase-space flow.

This analysis shows that the common and intuitive restoration practice in a 1:1 stripe pattern, where the planting pattern coincides with the ground modulation pattern, can result in a productive state but suffers from poor resilience to precipitation downshifts (droughts). By contrast, restoration in a rhombic pattern, which initiates the growth of the oblique modes, results in a productive and resilient state. More generally, these results suggest to disentangle the planting pattern from the ground modulation pattern and determine the former by identifying the growing (unstable) eigenmodes and analyzing the phase space they span. By focusing on the dynamical constraints that unstable states impose through their stable and unstable manifolds, judicious choices of planting patterns that result in functional ecosystem states can be made.

The phase-space information may also be used in managing ecosystems that have already been restored. The resilience of restored stripes can possibly be improved by spatial periodic biomass modulations, obtained by trimming or by managed grazing. This is because of the unstable rhombic solution whose stable manifold separates the basins of attraction of the bare-soil state and the stable rhombic pattern. Periodic biomass modulations will place the system in the attraction basin of the rhombic pattern by creating projections along the oblique eigenmodes.

These considerations can be generalized and applied to other contexts of human intervention in ecosystem dynamics, besides restoration, such as range management, regime-shift control, agroecology, and others. While they appear to rely on the availability of faithful mathematical models, empirical data analysis may prove to be a possible alternative when mathematical models are absent, such as the extraction of eigenmodes and phase-space elements from spatial Fourier transforms of satellite images. We note that the growing eigenmodes need not be spatially extended like the stripe and oblique modes in the restoration example. Contexts that involve localized structures, such as fronts in gradual regime shifts, can give rise to localized eigenmodes associated with translation symmetry [59] and possible front instabilities [34, 37, 91].

7.5 Conclusion

While pattern-formation phenomena in dryland ecosystems have been the subject of many theoretical and empirical studies [4, 13, 14, 57–59, 67, 84], many fewer studies have addressed the implications of pattern formation to ecosystem function in variable and disturbed environments [60], where state transitions may take place [41, 69], and in ecosystems subjected to human intervention. In Sect. 7.3 we considered several cases of bistable ecosystems, distinguishing between bistability of two uniform states and bistability of uniform and patterned states. In each case we discussed the implications of front dynamics to transitions from functional ecosystems states to less functional or dysfunctional states, emphasizing three aspects of front dynamics: single-front motion, front interactions, and front instabilities. The latter two aspects have received little attention even in the simplest bistability case of two uniform states [20]. The availability of fairly realistic models that are still simple enough to be mathematically tractable, such as the Namibian ecosystem model, should motivate additional studies. Because of the disparate length scales associated with biomass fronts (short) and water fronts (long) singular-perturbation methods may prove very useful in such studies [30, 36]. The relevance of homoclinic snaking in bistability ranges of uniform and patterned states to dryland vegetation has been demonstrated in several studies [11, 93, 94], including two-species models [47], but the physical and ecological factors that affect front pinning and determine the size of the homoclinic snaking range have remained unexplored.

Another intriguing and unstudied question is related to the similarity of pattern-formation phenomena in bistability ranges of uniform and patterned states and

bistability ranges of two uniform states. An example of such a phenomenon is a single gap of bare soil in otherwise uniform vegetation. Such a gap can be realized in a bistability range of uniform vegetation and periodic pattern as a hybrid state, but it can also be realized in a bistability range of uniform vegetation and bare soil as an outcome of repulsive front interactions. The capacity to determine which mechanism is at work in a given realization of a single gap is highly significant. In the former case rainfall fluctuations may drive the system outside the snaking range and induce a gradual shift to the less productive periodic gap pattern, which amounts to moderate desertification. In the latter case rainfall fluctuations may drive the system below the Maxwell point and induce a gradual shift to the unproductive bare-soil state, which amounts to severe desertification.

Although the significance of unstable states in ecosystem dynamics has already been stressed [35], the roles these states may play in planning human intervention have remained largely unexplored. An example of a significant problem that can be studied using an approach similar to that described for the restoration of degraded landscapes is range management in drought-prone ecosystems. Consider, for example, managing grazing in uniform grasslands. The disappearance of unstable uniform-vegetation solutions at low precipitation rates may induce collapse to bare soil rather than convergence to a periodic pattern, very much like the disappearance of unstable stripe solutions in the restoration problem. This suggests the management of grazing in spatial patterns, in order to locate the system in the basin of attraction of the periodic solution. Such management may result not only in the achievement of an ecosystem service—feeding livestock—but also in improved resilience to droughts.

Finally, the difficulty to conduct controlled laboratory experiments calls for the development of advanced data-analysis methods for remote sensing observations, geared to test model predictions of structural and dynamical fairy-circle characteristics, such as large-scale hexagonal order disrupted by penta-hepta defects [63] and hybrid-state transitions [22, 90, 93].

Acknowledgements Some of the results described here have been reported in earlier publications with additional colleagues, including Golan Bel, Stephan Getzin, Aric Hagberg, Lev Haim, Omer Tzuk, and Hezi Yizhaq. We gratefully acknowledge their contributions. The research leading to the results described in this chapter received funding from the Israel Science Foundation Grant 305/13.

References

1. Adeel, Z., Safriel, U., Niemeijer, D., et al.: Ecosystems and human well-being: Desertification synthesis. Technical Report of the Millennium Ecosystem Assessment, World Resources Institute, Washington, D.C. (2005)
2. Barbier, N., Couteron, P., Lefever, R., et al.: Spatial decoupling of facilitation and competition at the origin of gapped vegetation patterns. *Ecology* **89**, 1521–1531 (2008)
3. Bel, G., Hagberg, A., Meron, E.: Gradual regime shifts in spatially extended ecosystems. *Theor. Ecol.* **5**, 591–604 (2012)

4. Borgogno, F., D'Odorico, P., Laio, F., et al.: Mathematical models of vegetation pattern formation in ecohydrology. *Rev. Geophys.* **47**, RG1005 (2009)
5. Borthagaray, A.I., Fuentes, M.A., Marquet, P.A.: Vegetation pattern formation in a fog-dependent ecosystem. *J. Theor. Biol.* **265**(1), 18–26 (2010)
6. Chen, Y., Kolokolnikov, T., Tzou, J., et al.: Patterned vegetation, tipping points, and the rate of climate change. *Eur. J. Appl. Math.* **26**, 945–958 (2015)
7. Couillet, P., Lega, J., Houchmanzadeh, B., et al.: Breaking chirality in nonequilibrium system. *Phys. Rev. Lett.* **65**, 1352 (1990)
8. Cramer, M.D., Barger, N.N.: Are Namibian fairy circles the consequence of self-organizing spatial vegetation patterning? *PLoS One* **8**(8), e70,876 (2013)
9. Cramer, M.D., Barger, N.N., Tschinkel, W.R.: Edaphic properties enable facilitative and competitive interactions resulting in fairy circle formation. *Ecography* **40**, 1210–1220 (2017)
10. Cross, M.C., Greenside, H.: *Pattern Formation and Dynamics in Nonequilibrium Systems*. Cambridge University Press, Cambridge (2009)
11. Dawes, J.H.P., Williams, J.L.M.: Localised pattern formation in a model for dryland vegetation. *J. Math. Biol.* **73**, 1–28 (2015)
12. DeAngelis, D.L., Gross, L.J. (eds.): *Individual-Based Models and Approaches on Ecology: Concepts and Models*. Chapman and Hall, New York (1992)
13. DeAngelis, D.L., Yurek, S.: Spatially explicit modeling in ecology: A review. *Ecosystems* **20**(2), 284–300 (2017). <https://doi.org/10.1007/s10021-016-0066-z>
14. Deblauwe, V., Barbier, N., Couteron, P., et al.: The global biogeography of semi-arid periodic vegetation patterns. *Glob. Ecol. Biogeogr.* **17**, 715–723 (2008)
15. Dirzo, R., Young, H.S., Galetti, M., et al.: Defaunation in the anthropocene. *Science* **345**, 401–406 (2014)
16. D'Odorico, P., Bhattachan, A., Davis, K.F., et al.: Global desertification: Drivers and feedbacks. *Adv. Water Resour.* **51**, 326–344 (2013)
17. Duraiappah, A.K., Naeem, S.: *Ecosystems and human well-being: biodiversity synthesis*. Technical Report of the Millennium Ecosystem Assessment, World Resources Institute, Washington, DC. (2005)
18. Eldridge, D.J., Zaady, E., Shachak, M.: Infiltration through three contrasting biological soil crusts in patterned landscapes in the Negev, Israel. *J. Stat. Phys.* **148**, 723–739 (2012)
19. Ellis, E.C.: Ecology in an anthropogenic biosphere. *Ecol. Monogr.* **85**, 287–331 (2015)
20. Fernandez-Oto, C., Tlidi, M., Escaff, D., et al.: Strong interaction between plants induces circular barren patches: fairy circles. *Phil. Trans. R. Soc. A* **372**(2027), 20140009 (2014)
21. Field, C.B., Barros, V., Stocker, T.F., et al.: *Managing the risks of extreme events and disasters to advance climate change adaptation: a special report of the Intergovernmental Panel on Climate Change*. Technical Report, Cambridge University Press, Cambridge, UK, and New York, NY (2013)
22. Getzin, S., Wiegand, K., Wiegand, T., et al.: Adopting a spatially explicit perspective to study the mysterious fairy circles of Namibia. *Ecography* **38**, 1–11 (2015)
23. Getzin, S., Yizhaq, H., Bell, B., et al.: Discovery of fairy circles in Australia supports self-organization theory. *Proc. Natl. Acad. Sci.* **113**(13), 3551–3556 (2016)
24. Gilad, E., Von Hardenberg, J., Provenzale, A., et al.: Ecosystem engineers: from pattern formation to habitat creation. *Phys. Rev. Lett.* **93**, 098105 (2004)
25. Gilad, E., Shachak, M., Meron, E.: Dynamics and spatial organization of plant communities in water limited systems. *Theor. Popul. Biol.* **72**, 214–230 (2007)
26. Gilad, E., Von Hardenberg, J., Provenzale, A., et al.: A mathematical model for plants as ecosystem engineers. *J. Theor. Biol.* **244**, 680 (2007)
27. Goldstein, R.E., Muraki, D.J., Petrich, D.M.: Interface proliferation and the growth of labyrinths in a reaction-diffusion system. *Phys. Rev. E* **53**, 3933–3957 (1996)
28. Gowda, K., Riecke, H., Silber, M.: Transitions between patterned states in vegetation models for semiarid ecosystems. *Phys. Rev. E* **89**, 022,701 (2014)
29. Grimm, V., Railsback, S.F.: *Individual-based Modeling and Ecology*. Princeton University Press, Princeton (2005)

30. Hagberg, A., Meron, E.: Complex patterns in reaction diffusion systems: a tale of two front instabilities. *Chaos* **4**, 477–484 (1994)
31. Hagberg, A., Meron, E.: From labyrinthine patterns to spiral turbulence. *Phys. Rev. Lett.* **72**, 2494–2497 (1994)
32. Hagberg, A., Meron, E.: Pattern formation in non-gradient reaction diffusion systems: the effects of front bifurcations. *Nonlinearity* **7**, 805–835 (1994)
33. Hagberg, A., Meron, E.: The dynamics of curved fronts: beyond geometry. *Phys. Rev. Lett.* **78**, 1166–1169 (1997)
34. Hagberg, A., Meron, E., Rubinstein, I., et al.: Controlling domain patterns far from equilibrium. *Phys. Rev. Lett.* **76**, 427–430 (1996)
35. Hastings, A.: The key to long-term ecological understanding? *Trends Ecol. Evol.* **19**, 39–45 (2004)
36. van Heijster, P., Doelman, A., Kaper, T.J., et al.: Front interactions in a three-component system. *SIAM J. Appl. Dyn. Syst.* **9**(2), 292–332 (2010)
37. Hilker, F.M., Lewis, M.A., Seno, H., et al.: Pathogens can slow down or reverse invasion fronts of their hosts. *Biol. Invasions* **7**(5), 817–832 (2005)
38. Homburg, A.J., Sandstede, B.: Homoclinic and heteroclinic bifurcations in vector fields. In: *Handbook of Dynamical Systems*, vol. 3, pp. 379–524. Elsevier, Amsterdam (2010)
39. Ikeda, H., Mimura, M., Nishiura, Y.: Global bifurcation phenomena of travelling wave solutions for some bistable reaction-diffusion systems. *Nonlinear Anal. Theory Methods Appl.* **13**, 507–526 (1989)
40. Juergens, N.: The biological underpinnings of Namib Desert fairy circles. *Science* **339**(6127), 1618–1621 (2013)
41. Kéfi, S., Vishwesh, G., Brock, W.A.: Early warning signals of ecological transitions: methods for spatial patterns. *Plos One* **9**, e92097 (2014)
42. Kinast, S., Zelnik, Y.R., Bel, G., et al.: Interplay between turing mechanisms can increase pattern diversity. *Phys. Rev. Lett.* **112**, 078701 (2014)
43. Klausmeier, C.A.: Regular and irregular patterns in semiarid vegetation. *Science* **284**, 1826–1828 (1999)
44. Kletter, A.Y., von Hardenberg, J., Meron, E.: Ostwald ripening in dryland vegetation. *Commun. Pure Appl. Anal.* **11**, 261–273 (2012)
45. Knobloch, E.: Spatially localized structures in dissipative systems: open problems. *Nonlinearity* **21**, T45 (2008)
46. Knobloch, E.: Spatial localization in dissipative systems. *Ann. Rev. Condens. Matter Phys.* **6**(1), 325–359 (2015)
47. Kyriazopoulos, P., Jonathan, N., Meron, E.: Species coexistence by front pinning. *Ecol. Complex.* **20**, 271–281 (2014)
48. Lefever, R., Lejeune, O.: On the origin of tiger bush. *Bull. Math. Biol.* **59**, 263–294 (1997)
49. Lejeune, O., Couteron, P., Lefever, R.: Short range co-operativity competing with long range inhibition explains vegetation patterns. *Acta Oecol.* **20**(3), 171–183 (1999)
50. Lejeune, O., Tlidi, M., Lefever, R.: Vegetation spots and stripes: dissipative structures in arid landscapes. *Int. J. Quantum Chem.* **98**, 261–271 (2004)
51. Maestre, F.T., Eldridge, D.J., Soliveres, S., et al.: Structure and functioning of dryland ecosystems in a changing world. *Annu. Rev. Ecol. Evol. Syst.* **47**(1), 215–237 (2016)
52. Marten, G.G.: *Human Ecology - Basic Concepts for Sustainable Development*. Earthscan Publications, London (2001)
53. Marts, B., Hagberg, A., Meron, E., et al.: Bloch-front turbulence in a periodically forced Belousov-Zhabotinsky reaction. *Phys. Rev. Lett.* **93**(108305), 1–4 (2004)
54. Mau, Y., Hagberg, A., Meron, E.: Spatial periodic forcing can displace patterns it is intended to control. *Phys. Rev. Lett.* **109**, 034102 (2012)
55. Mau, Y., Haim, L., Hagberg, A., et al.: Competing resonances in spatially forced pattern-forming systems. *Phys. Rev. E* **88**, 032,917 (2013)
56. Mau, Y., Haim, L., Meron, E.: Reversing desertification as a spatial resonance problem. *Phys. Rev. E* **91**, 012,903 (2015)

57. Meron, E.: Modeling dryland landscapes. *Math. Model. Nat. Phenom.* **6**, 163–187 (2011)
58. Meron, E.: Pattern-formation approach to modelling spatially extended ecosystems. *Ecol. Model.* **234**, 70–82 (2012)
59. Meron, E.: *Nonlinear Physics of Ecosystems*. CRC Press, Taylor & Francis Group, Boca Raton (2015)
60. Meron, E.: Pattern formation – a missing link in the study of ecosystem response to environmental changes. *Math. Biosci.* **271**, 1–18 (2016)
61. Mimura, M., Tohma, M.: Dynamic coexistence in a three-species competition–diffusion system. *Ecol. Complex.* **21**, 215–232 (2015)
62. Petraitis, P.: *Multiple Stable States in Natural Ecosystems*. Oxford University Press, Oxford (2013)
63. Pismen, L.: *Patterns and Interfaces in Dissipative Dynamics*. Springer Series in Synergetics. Springer, Berlin (2006)
64. Pomeau, Y.: Front motion, metastability and subcritical bifurcations in hydrodynamics. *Phys. D* **23**, 3 (1986)
65. Ravi, S., Wang, L., Kaseke, K.F., et al.: Ecohydrological interactions within “fairy circles” in the Namib Desert: revisiting the self-organization hypothesis. *J. Geophys. Res. Biogeosci.* **122**(2), 405–414 (2017)
66. Reynolds, J.F., Smith, D.M.S., Lambin, E.F., et al.: Global desertification: building a science for dryland development. *Science* **316**(5826), 847–851 (2007)
67. Rietkerk, M., van de Koppel, J.: Regular pattern formation in real ecosystems. *Trends Ecol. Evol.* **23**(3), 169–175 (2008)
68. Rietkerk, M., Boerlijst, M.C., van Langevelde, F., et al.: Self-organization of vegetation in arid ecosystems. *Am. Nat.* **160**, 524–530 (2002)
69. Rietkerk, M., Dekker, S.C., de Ruiter, P.C., van de Koppel, J.: Self-organized patchiness and catastrophic shifts in ecosystems. *Science* **305**, 1926–1929 (2004)
70. Scheffer, M., Bascompte, J., Brock, W.A., et al.: Early-warning signals for critical transitions. *Nature* **461**, 387–393 (2009)
71. Scheffer, M., Carpenter, S.R.: Catastrophic regime shifts in ecosystems: linking theory to observation. *Trends Ecol. Evol.* **18**, 648–656 (2003)
72. Scheffer, M., Carpenter, S., Foley, J.A., et al.: Catastrophic shifts in ecosystems. *Nature* **413**, 591–596 (2001)
73. Sherratt, J.A.: An analysis of vegetation stripe formation in semi-arid landscapes. *J. Math. Biol.* **51**(2), 183–197 (2005). <https://doi.org/10.1007/s00285-005-0319-5>
74. Sherratt, J.A.: Pattern solutions of the Klausmeier model for banded vegetation in semiarid environments, V: the transition from patterns to desert. *SIAM J. Appl. Math.* **73**, 1347–1367 (2013)
75. Sherratt, J.A.: When does colonisation of a semi-arid hillslope generate vegetation patterns? *J. Math. Biol.* **73**, 199–226 (2016)
76. Sherratt, J.A., Synodinos, A.D.: Vegetation patterns and desertification waves in semi-arid environments: mathematical models based on local facilitation in plants. *Discrete Contin. Dynam. Systems B* **17**(8), 2815–2827 (2012)
77. Shnerb, N.M., Sarah, P., Lavee, H., et al.: Reactive glass and vegetation patterns. *Phys. Rev. Lett.* **90**, 0381011 (2003)
78. Siero, E., Doelman, A., Eppinga, M.B., et al.: Striped pattern selection by advective reaction-diffusion systems: resilience of banded vegetation on slopes. *Chaos* **25**(3), 036411 (2015)
79. Siteur, K., Siero, E., Eppinga, M.B., et al.: Beyond Turing: The response of patterned ecosystems to environmental change. *Ecol. Complex.* **20**(0), 81–96 (2014)
80. Siteur, K., Eppinga, M.B., Doelman, A., et al.: Ecosystems off track: rate-induced critical transitions in ecological models. *Oikos* **125**, 1689–1699 (2016)
81. Stone, L., Weisburd, R.S.J.: Positive feedback in aquatic ecosystems. *Trends Ecol. Evol.* **7**, 263–267 (2016)
82. Strogatz, S.H.: *Nonlinear Dynamics and Chaos: With Applications to Physics, Biology, Chemistry, and Engineering*. Westview Press, Boulder (2001)

83. Tarnita, C., Bonachela, J.A., Sheffer, E., et al.: A theoretical foundation for multi-scale regular vegetation patterns. *Nature* **541**, 398–401 (2017)
84. Tongway, D.J., Valentin, C., Seghieri, J., et al. (eds.): *Banded Vegetation Patterning in Arid and Semiarid Environments: Ecological Processes and Consequences for Management*. Ecological Studies, vol. 149. Springer, Basel (2001)
85. Tschinkel, W.: The life cycle and life span of Namibian fairy circles. *PLoS One* **7**(6), e38056 (2012)
86. Valentine, C., d’Herbes, J., Poesen, J.: Soil and water components of banded vegetation patterns. *Catena* **37**, 1–24 (1999)
87. van der Stelt, S., Doelman, A., Hek, G.M., et al.: Rise and fall of periodic patterns for a generalized Klausmeier–Gray–Scott model. *J. Nonlinear Sci.* **23**, 39–95 (2013)
88. Vohland, K., Barry, B.: A review of in situ rainwater harvesting (RWH) practices modifying landscape functions in African drylands. *Agric. Ecosyst. Environ.* **131**, 119–127 (2009)
89. von Hardenberg, J., Meron, E., Shachak, M., et al.: Diversity of vegetation patterns and desertification. *Phys. Rev. Lett.* **89**, 198101 (2001)
90. Wiegand, T., Kissling, W.D., Cipriotti, P.A., et al.: Extending point pattern analysis for objects of finite size and irregular shape. *J. Ecol.* **94**(4), 825–837 (2006)
91. Zelnik, Y.R., Meron, E.: Regime shifts by front dynamics. *Ecol. Indic.* **94**, 544–552 (2018). <https://doi.org/10.1016/j.ecolind.2017.10.068>
92. Zelnik, Y.R., Kinast, S., Yizhaq, H., et al.: Regime shifts in models of dryland vegetation. *Philos. Trans. R. Soc. A* **371**, 20120358 (2013)
93. Zelnik, Y.R., Meron, E., Bel, G.: Gradual regime shifts in fairy circles. *Proc. Natl. Acad. Sci.* **112**, 12,327–12,331 (2015)
94. Zelnik, Y.R., Meron, E., Bel, G.: Localized states qualitatively change the response of ecosystems to varying conditions and local disturbances. *Ecol. Complex.* **25**, 26–34 (2016)
95. Zelnik, Y.R., Uecker, H., Feudel, U., et al.: Desertification by front propagation? *J. Theor. Biol.* **418**, 27–35 (2017)
96. Zelnik, Y.R., Gandhi, P., Knobloch, E., et al.: Implications of tristability in pattern-forming ecosystems. *Chaos Interdiscip. J. Nonlinear Sci.* **28**(3), 033609 (2018)